

Saturation of interband absorption in graphene

F.T. Vasko*

Institute of Semiconductor Physics, NAS of Ukraine, Pr. Nauky 41, Kiev, 03028, Ukraine

(Dated: October 29, 2018)

The transient response of an intrinsic graphene, which is caused by the ultrafast interband transitions, is studied theoretically for the range of pumping correspondent to the saturated absorption regime. Spectral and temporal dependencies of the photoexcited concentration as well as the transmission and relative absorption coefficients are considered for mid-IR and visible (or near-IR) spectral regions at different durations of pulse and broadening energies. The characteristic intensities of saturation are calculated and the results are compared with the experimental data measured for the near-IR lasers with a saturable absorber. The negative absorption of a probe radiation during cascade emission of optical phonons is obtained.

PACS numbers: 78.47.jb, 78.67.Wj, 42.65.-k

I. INTRODUCTION

The character of nonlinear response under the ultrafast interband excitation of an intrinsic graphene is determined by a several physical processes which are dependent on conditions of pumping. Under a low excitation level, when the one-photon transitions take place, the energy relaxation and recombination of photoexcited carriers were studied with the use of the time-resolved pump-probe measurements, see experimental data and theoretical discussions in Refs. 1 and 2, respectively. Under an extremely high pumping, the multi-quantum transitions, which cause the harmonics generation and the hybridization of electron-hole states, take place. This regime is not investigated completely for graphene, see general consideration for bulk materials or quantum wells in Sects. 10 and 56 of Ref. 3. The nonlinear response is also possible within the single-photon approach because the Rabi oscillations of coherent response should take place in graphene if a pulse duration is less 100 fs. [4] Beside of this, the nonlinear regime of energy relaxation and recombination due to the Pauli blocking effect takes place if the photo-generation rate is comparable to the energy relaxation or recombination rates. A saturation of transient absorption, which have been investigated recently, [5, 6] is the most important manifestation of such a regime. It is because this phenomenon was exploited for realization of an ultrafast laser with a graphene saturable absorber in the telecommunication spectral region. To the best of our knowledge, a complete theoretical treatment of the saturation mechanism is not performed yet and an investigation of this phenomena is timely now.

In this paper, we consider the temporal nonlinear evolution of carriers under photoexcitation by the ultrafast pulses in mid-IR and visible (or near-IR) spectral regions. For the mid-IR pump, one can neglect the relaxation and recombination processes (the quasielastic relaxation due to acoustic phonons remains ineffective up to nanosec-

onds) and the transient distribution of nonequilibrium carriers is determined by the broadening of interband transitions due to an elastic scattering and by the parameters of excitation. For the excitation energies, $\hbar\Omega$, above the optical phonon energy, $\hbar\omega_\eta$ ($\eta = \Gamma, K$ labels the phonon modes correspondent to the intra- and intervalley transitions), when a cascade emission of the optical phonons dominates in relaxation, the transient distribution transforms into a set of peaks. The effective electron-hole recombination takes place if the lowest peak is placed around the half-energy of optical phonon, $\hbar\omega_\eta/2$. So that, the character of response modifies essentially if the frequency Ω varies over the ω_η -range.

The saturation process is described within the framework of the temporally local approach, when the decoherence time (which determines the broadening of the interband transitions) is shorter in comparison with the duration of pumping. Spectral and temporal dependencies of the photoexcited concentration and the response on the probe radiation (transmission and absorption coefficients) are presented. The thresholds for saturation of response are estimated to be about 0.2 MW/cm², 60 MW/cm², and 0.6 GW/cm² for $\hbar\Omega \sim 0.12, 0.8, \text{ and } 1.5$ eV, respectively (mid-IR, near-IR, and visible spectral regions). These results are dependent on the decoherence and relaxation mechanisms and the electrodynamics conditions. Their are discussed in comparison with the experimental data for the near-IR pumping case [5, 6]. Conditions for the transient negative absorption of a probe radiation during cascade emission of optical phonons are also analyzed (this phenomenon under a steady-state pumping was considered recently [7] in connection with a possibility of the THz lasing effect).

The consideration below is organized as follows. The temporally local approach for description of the response of photoexcited carriers is developed in Sec. II. Spectral and temporal dependencies of the response are described in Sects. III and IV for the cases of excitation in mid-IR and visible (or near-IR) spectral regions, respectively. A discussion of experimental data, the list of assumptions used, and concluding remarks are given in the last section. In Appendix we consider the mechanism of sat-

*Electronic address: ftvasko@yahoo.com

uration caused by the collisionless Rabi oscillations.

II. TEMPORALLY LOCAL APPROACH

Since the symmetry of the energy spectrum and scattering processes for electrons and holes in an intrinsic graphene, we describe the phenomena under consideration by the same distribution functions for the both types of carriers, f_{pt} . According to Refs. 2b and 4, the kinetic equation for f_{pt} takes form:

$$\frac{df_{pt}}{dt} = \nu_{pt}(1 - 2f_{pt}) + J(f_t|p) \quad (1)$$

and it should be solved with the initial condition $f_{pt \rightarrow \infty} = 0$. Here $J(f_t|p)$ is the collision integral, which is described the relaxation and recombination processes, and ν_{pt} is the interband generation rate due to the in-plane electric field $\mathbf{E}w_t \exp(-i\Omega t) + c.c.$, where \mathbf{E} is the field strength, Ω is the pumping frequency, and w_t is the envelope form-factor of pulse with duration $2\tau_p$ centered at $t = 0$. Supposing that τ_p exceeds the dephasing time, we have used in Eq. (1) the temporally local approach with the separated filling factor, $(1 - 2f_{pt})$, and with the rate of photoexcitation:

$$\nu_{pt} = \nu_R w_t^2 \Delta \left(\frac{2\nu p - \hbar\Omega}{\gamma} \right), \quad \nu_R = \frac{\pi(eEv/\Omega)^2}{\hbar\gamma}. \quad (2)$$

Here $v = 10^8$ cm/s is the velocity of neutrino-like quasi-particles, 2γ is the broadening of the interband excitation described by the phenomenological factor $\Delta(z)$. Below we consider the Lorentzian lineshape of photoexcitation, when $\Delta(z) = [\pi(1 + z^2)]^{-1}$ and the Gaussian temporal envelope $w_\tau = \sqrt{2/\pi} \exp[-(t/\tau_p)^2]$.

The solution of Eq. (1) determines both the photoinduced concentration, which given by the standard formula

$$n_t = \frac{2}{\pi\hbar^2} \int_0^\infty dp p f_{pt}, \quad (3)$$

and the transient response on a probe radiation of frequency ω ($\propto \exp(-i\omega t)$), which is described by the dynamic conductivity $\sigma_{\omega t}$. For the collisionless case $\hbar\omega/\gamma \gg 1$, when the parametric dependency on time takes place, [9] the real part of $\sigma_{\omega t}$ is written as follows:

$$\text{Re}\sigma_{\omega t} = \frac{e^2}{4\hbar}(1 - 2f_{p\omega,t}), \quad (4)$$

where $p_\omega = \hbar\omega/v$. The imaginary part of $\sigma_{\omega t}$ is determined through $\text{Re}\sigma_{\omega t}$ with the use of the dispersion relation and one can check that the carrier-induced contribution to $\text{Im}\sigma_{\omega t}$ appears to be weak in comparison with (4) for the peak-like distributions of carriers considered below. Thus, the only filling factor in $\text{Re}\sigma_{\omega t}$ is

responsible for the nonlinear behavior of the response under consideration.

We restrict ourselves by the the geometry of normal propagation of radiation. The relative absorption of graphene sheet, $\xi_{\omega t}$, as well as the reflection and transmission coefficients, $R_{\omega t}$ and $T_{\omega t}$, are determined through $\sigma_{\omega t}$. Since the energy conservation requirement, [8]

$$R_{\omega t} + T_{\omega t} + \xi_{\omega t} = 1, \quad (5)$$

we consider below only the absorption and transmission coefficients:

$$\xi_{\omega t} \simeq \frac{16\pi}{\sqrt{\epsilon}c} \frac{\text{Re}\sigma_{\omega t}}{|1 + \sqrt{\epsilon} + 4\pi\sigma_{\omega t}/c|^2} \approx \xi_m(1 - 2f_{p\omega,t}),$$

$$T_{\omega t} \simeq \frac{4\sqrt{\epsilon}}{|1 + \sqrt{\epsilon} + 4\pi\sigma_{\omega t}/c|^2} \approx \frac{T_m}{(1 - af_{p\omega,t})^2}. \quad (6)$$

Here $\sqrt{\epsilon}$ is the refraction index of a thick substrate (for SiO₂ substrate $\sqrt{\epsilon} \simeq 1.45$ and dispersion of ϵ can be neglected) and we approximately separated the carrier contributions using the coefficients $\xi_m \approx 4\pi\alpha/[\sqrt{\epsilon}(1 + \sqrt{\epsilon})]$, $T_m \approx 4\sqrt{\epsilon}/(1 + \sqrt{\epsilon} + \pi\alpha)^2$, and $a \approx 2\pi\alpha/(1 + \sqrt{\epsilon} + \pi\alpha)$ with $\alpha = e^2/\hbar c$. Notice, that the negative absorption regime $\xi_{\omega t} < 0$ takes place if $f_{p\omega,t} > 1/2$, under the population inversion condition (see discussion in Sec. IV).

At $\omega = \Omega$ these relations describe the propagation of pumping pulse with the time-dependent intensity $S w_t^2$, where S is the maximal intensity. Performing the averaging of (6) over the pulse duration one obtains

$$\left| \frac{\xi_S}{T_S} \right| = \int_{-\infty}^{\infty} \frac{dt}{\tau_p} w_t^2 \left| \frac{\xi_{\Omega t}}{T_{\Omega t}} \right|, \quad (7)$$

where we used $\int_{-\infty}^{\infty} dt w_t^2/\tau_p = 1$. Below we solve Eq. (1) and analyze the responses (6) and (7) for different parameters of pump and probe radiations.

III. MID-IR EXCITATION

We consider here the mid-IR pumping case when the energy relaxation of carriers is ineffective and $J(f_t|p)$ in Eq. (1) can be neglected. As a result, the solution of the problem (1) takes form:

$$f_{pt} = \int_{-\infty}^t dt' \nu_{pt'} \exp\left(-2 \int_{t'}^t d\tau \nu_{p\tau}\right). \quad (8)$$

Evolution of such a distribution from zero value at $t \ll -\tau_p$ to the saturated peak with the maximal value $f_{max} = 1/2$ is shown in Fig. 1a versus dimensionless time and energy at the pumping intensity $S = 1$ MW/cm². Temporal dependencies of $f_{p\omega t}$ at different S are shown in Fig. 1b. These calculations were performed for $\hbar\Omega \simeq 120$

meV (pumping by CO₂-laser), the pulse duration $2\tau_p \simeq 1$ ps, and the broadening energy $\gamma \simeq 6$ meV which is in agreement with the mobility data for the case of elastic scattering. [9] The temporally-dependent photoinduced concentration n_t is plotted Fig. 1c for the same parameters. The saturated concentration versus intensity, which is attained at $t > \tau_p$, is presented for $\gamma = 6$ and 12 meV in Fig. 1d. These dependencies can be fitted as

$$n_S \approx \frac{bS}{1 + S/S_n}, \quad (9)$$

where $b \simeq 6$ or 12.2 MW^{-1} [n_S is measured in 10^{11} cm^{-2}] and $S_n \simeq 1.76$ or 10 MW/cm^2 for and $\gamma = 6$ or 12 meV, respectively.

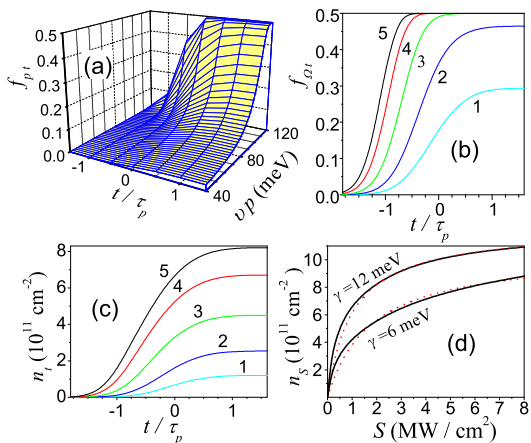


FIG. 1: (Color online) (a) Photoexcited distribution f_{pt} versus energy vp and dimensionless time, t/τ_p at mid-IR pumping level $S = 1 \text{ MW/cm}^2$. (b) Temporal evolution of $f_{\Omega t} \equiv f_{p\Omega t}$ at $S = 0.1, 0.3, 1, 3,$ and 6 MW/cm^2 (marked as 1-5). (c) Photoinduced concentration versus t/τ_p for the same conditions as in panel (b). (d) Concentration n_S at $t/\tau_p \rightarrow \infty$ versus S for the different broadening energies γ . Dotted curves are correspondent to the fit (9).

The relative absorption and transmission coefficients of a probe radiation of frequency ω are determined through $f_{p\omega t}$ according to Eqs. (6). Spectral and temporal dependencies of $\xi_{\omega t}$ are shown in Fig. 2a for the conditions used in Fig. 1a. Since $af_{p\omega t} \ll 1$, the peak of relative transmission $T_{\omega t}/T_m$ resembles $f_{p\omega t}$ presented in Fig. 1a. Here $T_m \simeq 0.95$ is the transmission coefficient without for non-doped graphene. The temporally-dependent relative absorption and transmission at the pumping frequency Ω and at different S are presented in Figs. 2b and 2c, respectively. The saturated values of ξ_S/ξ_m and T_S versus intensity are plotted in the upper and lower panels of Fig. 2d for the parameters used in Fig. 1d (ξ_S and T_S have only a weak dependency on γ). These curves can be fitted as

$$\xi_S \approx \frac{\xi_m}{1 + S/\bar{S}}, \quad T_S \approx T_m + \frac{hS}{1 + S/\bar{S}}, \quad (10)$$

where $\bar{S} \approx 0.2 \text{ MW/cm}^2$ and $h \approx 0.09 \text{ cm}^2/\text{MW}$. The saturation of ξ_S and T_S takes place at lower threshold intensities in comparison to n_S , c. f. Figs. 1c and 2d, 2e. Thus, for the pumping range $\geq 1 \text{ MW/cm}^2$ the one-photon absorption is suppressed and a damage of graphene by mid-IR radiation with $\tau_p \lesssim 1$ ps is not possible.

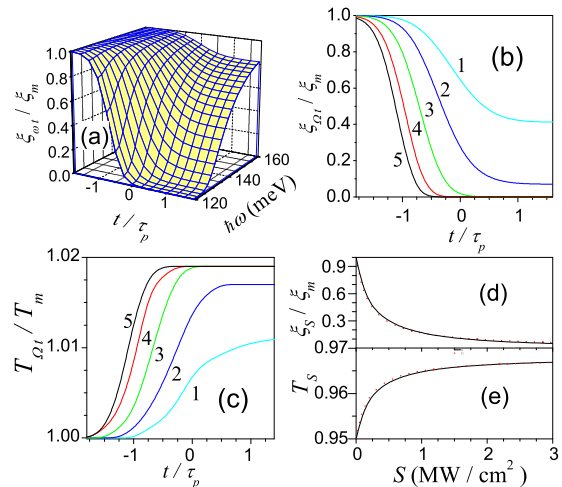


FIG. 2: (Color online) (a) Spectral and temporal dependencies of relative absorption, $\xi_{\omega t}$ at $S = 1 \text{ MW/cm}^2$. (b) Temporal evolution of $\xi_{\Omega t}$ at S used in Fig. 1b (marked). (c) The same as in panel (b) for transmission, $T_{\Omega t}$. (d) Averaged over pulse absorption and transmission coefficients (upper and lower panels, respectively) versus S [dashed curves are correspondent to Eq. (10)].

IV. CASCADE EMISSION EFFECT

In this section we consider the photoexcitation by visible and near-IR radiation, when the cascade emission of optical phonons should be taken into account in Eq. (1). For the temperatures below the optical phonon energies, the spontaneous emission processes are only essential and the collision integral is given by the finite-difference form (see evaluation in Refs. 2b and 10)

$$J(f_t|p) = \sum_{\eta} [\nu_{p+p_{\eta}} (1 - f_{pt}) f_{p+p_{\eta}t} - \nu_{p-p_{\eta}} (1 - f_{p-p_{\eta}t}) f_{pt} - \tilde{\nu}_{p_{\eta}-p} f_{p_{\eta}-pt} f_{pt}]. \quad (11)$$

Here $\eta = \Gamma$, K is correspondent to the intra- and intervalley transitions with the energy transfer, $\hbar\omega_{\eta}$, and the momentum transfer, $p_{\eta} = \hbar\omega_{\eta}/v$. The last contribution of Eq. (11) is responsible for the recombination process while the first and second terms describe the interband cascade relaxation of carriers. The relaxation rates ν_p and $\tilde{\nu}_p$ are proportional to the density of states, $\nu_p \approx \tilde{\nu}_p \approx \theta(p)v_{\eta}p/\hbar$, where the characteristic velocities

$\nu_{\Gamma,K}$ can be estimated crudely as $\nu_K \approx 2 \times 10^6$ cm/s and $\nu_{\Gamma} \approx 10^6$ cm/s. [10] Thus, the K -mode emission gives a dominant contribution to the relaxation process; moreover, the only interband recombination is possible in the passive region, $0 < \nu p < \hbar\omega_K = 170$ meV. Below we neglect other relaxation processes, so that a peak-like transient distribution of carriers takes place due to the negligible phonon dispersion and a narrow distribution of photoexcited carriers, under the condition $\gamma \ll \hbar\omega_K$. For the sake of simplicity, the cases of effective or suppressed recombination, when the lower peak in the passive region is placed around or outside the energy $\hbar\omega_K$ are considered. It is convenient to analyze calculations for the near-IR and visible pumping cases separately.

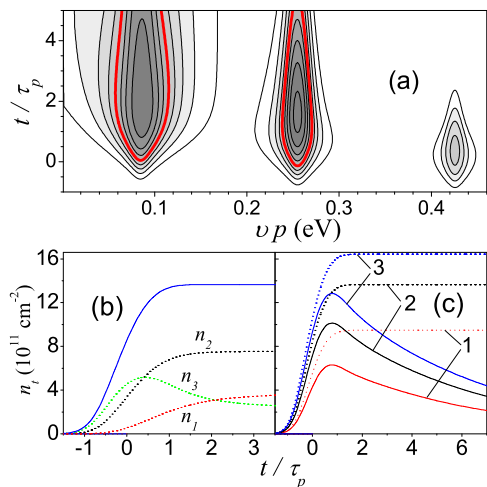


FIG. 3: (Color online) (a) Contour plots of photoexcited distributions f_{pt} versus energy and time for pulse duration $2\tau_p = 0.6$ ps at pumping level 200 MW/cm 2 and $\hbar\Omega = 850$ meV. (b) Transient evolution of concentration n_t and populations of peaks around ~ 43 , 213 , and 383 meV (marked as n_1 , n_2 , and n_3 , respectively), for the same conditions as in panel (a). (c) Evolution of n_t for pumping levels $S = 100$, 200 , and 300 MW/cm 2 (marked as 1, 2, and 3). Solid and dashed curves are plotted for $\hbar\Omega = 850$ meV and 765 meV.

A. Near-IR pumping

First, we consider the three-step cascade processes under the near-IR pumping with wavelengths around ~ 1.5 μm and the pulse duration determined by $\tau_p = 0.3$ ps. We consider the regimes of the enhanced or suppressed recombination supposing $\hbar\Omega = 850$ meV or 765 meV. For this energy region, the broadening of photoexcited peak is taken as $\gamma \simeq 18$ meV, so that $\hbar/\gamma \ll \tau_p$. The numerical solution of Eq. (1) with the collision integral (11) is performed with the use of the temporal iterations [11] at different S . Figure 2a shows the contour plot of the three-peak distribution function f_{pt} for the case of efficient recombination ($\hbar\Omega = 850$ meV) at $S = 200$

MW/cm 2 . The carrier concentrations over the peaks 1-3 and the total concentration n_t given by Eq. (3) are shown in Fig. 3b for the same parameters as in Fig. 1a. Since the relaxation rate in Eq. (11) is proportional to the density of states, $\nu_p \propto p$, the bottleneck effect takes place under the transition between the second and third peaks and n_2 exceeds $n_{1,3}$. The transient evolution of concentration for different S is shown in Fig. 3c where the maximal concentration exceeds 10^{12} cm $^{-2}$ at $t \sim \tau_p$ and $S \geq 0.3$ GW/cm 2 . During the further evolution, n_t decays due to the recombination process. The case of the suppressed recombination ($\hbar\Omega = 765$ meV) is different because of, first, the peaks are shifted below (about 43 meV) and, second, the decreasing of f_{pt} and n_t due to recombination is absent. The saturated concentrations (dashed curves in Fig. 3c) exceed the peak concentrations (solid curves in Fig. 3c) by factor ~ 1.3 . Note, that n_t decreases with increasing of γ at fixed S (not shown in Fig. 3).

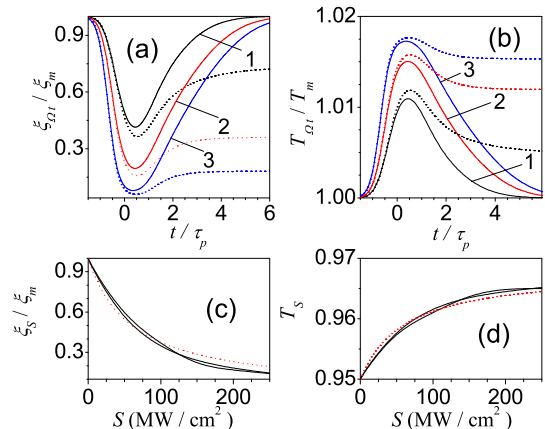


FIG. 4: (Color online) (a) Transient evolution of relative absorption for $\hbar\Omega = 850$ and 765 meV (solid and dotted curves, respectively) at $S = 50, 100$ and 200 MW/cm 2 (marked as 1-3). (b) The same as in panel (a) for transmission coefficient. (c) Averaged over pulse absorption versus S [dashed curve is correspondent to Eq. (9)]. (d) The same as in panel (c) for transmission coefficient.

Transient evolutions of the absorption and transmission coefficients given by Eq. (6) are shown in Figs. 4a and 4b at the different pumping frequencies Ω (solid and dashed curves) and at different S . For $t/\tau_p \leq 0.5$, the temporal evolution of $\xi_{\Omega t}$ and $T_{\Omega t}$ do not depend on the character of recombination. For $t/\tau_p \lesssim 1.5$ this evolution is completely different: a quenching of photoreponse or a steady-state contribution take place for the effective or suppressed recombination cases. At $S \geq 300$ MW/cm 2 and $t/\tau_p \sim 0$ one obtains the saturated absorption around $\xi_{\Omega t} \sim 0.1$. The negative absorption takes place for a probe radiation with $\hbar\omega$ around the first and second peaks. It is because $f_{p\omega t} > 1/2$, see Eq. (4) and the contour plot in Fig. 3, where the regions of negative absorption are separated by the thick (red) curves. Thus,

the negative absorption (and a possible stimulated emission of mid-IR radiation) is realized at $S \geq 100 \text{ MW/cm}^2$ during time intervals $t \lesssim 5\tau_p$.

The absorption and transition coefficients averaged over pulse duration according to Eq. (7) are shown in Figs. 4c and 4d. Since the transient response at $|t| \lesssim \tau_p$ does not depend on the recombination mechanism (see Figs. 3c, 4a, and 4b), the variation of ξ_S and T_S with $\hbar\Omega$ is less than 5%. These dependencies can be fitted by Eq. (10) with the characteristic intensity $\bar{S} \approx 60 \text{ MW/cm}^2$ and the coefficient $h \approx 0.3 \text{ cm}^2/\text{GW}$.

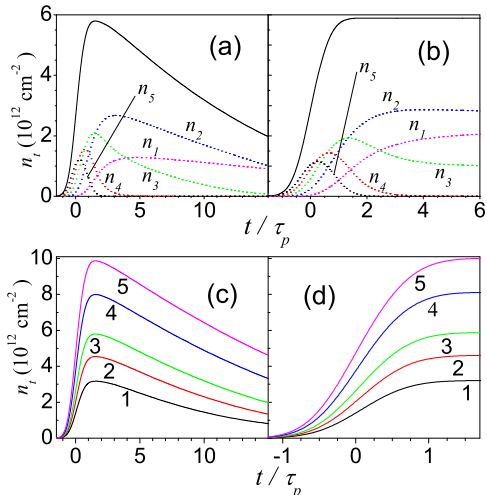


FIG. 5: (Color online) (a) Transient evolution of concentration n_t and populations of peaks around $\sim 0.09, 0.26, 0.43, 0.6,$ and 0.77 eV (marked as n_{1-5} , respectively) for pulse duration $2\tau_p = 0.4 \text{ ps}$ at pumping level 0.4 GW/cm^2 and $\hbar\Omega = 1.53 \text{ eV}$. (b) The same as in panel (a) at $\hbar\Omega = 1.615 \text{ eV}$ for peak's positions $\sim 0.13, 0.3, 0.47, 0.64,$ and 0.81 eV marked as n_{1-5} . (c) Evolution of n_t for pumping levels $S = 0.2, 0.3, 0.4, 0.6$ and 0.8 GW/cm^2 (marked as 1-5, respectively) for $\hbar\Omega = 1.53 \text{ eV}$. (d) The same as in panel (c) for $\hbar\Omega = 1.615 \text{ eV}$.

B. Visible pumping

Next, we consider the visible light pumping, with wavelengths around $\sim 0.75 \mu\text{m}$, using the pulse duration $2\tau_p = 0.4 \text{ ps}$ and the broadening $\gamma \approx 34 \text{ meV}$ (so that $\hbar/\gamma \ll \tau_p$). Supposing $\hbar\Omega = 1.53$ and 1.615 eV for the enhanced and suppressed recombination regimes one arrive to the distribution function formed during the five-step cascade process. Transient evolutions of the concentrations over the peaks 1-5 and of the total concentration n_t at $S = 0.4 \text{ GW/cm}^2$ are shown in Figs. 5a and 5b for the cases of enhanced and suppressed recombination, respectively. Similarly to the near-IR pumping case, the upper peak concentrations decrease fast at $t > \tau_p$ and a maximal population of the second peak takes place due to the bottleneck effect. Once again, at $t < \tau_p$ the shapes of n_t are the same for the both cases. At $t > \tau_p$ a quenching

of n_t due to recombination takes place in Fig. 5a while there is no a decreasing of n_t in Fig. 5b. The temporal dependencies of concentration for different S are shown in Figs. 5c and 5d for the two recombination regimes under consideration. The maximal concentration range up to 10^{13} cm^{-2} at $t \sim \tau_p$ and $S \approx 1 \text{ GW/cm}^2$.

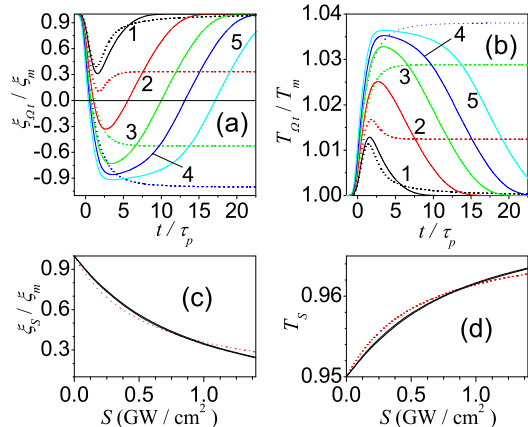


FIG. 6: (Color online) (a) Transient evolution of relative absorption for $\hbar\Omega = 1.53$ and 1.615 eV , (solid and dotted curves respectively) at $S = 0.2, 0.4, 0.6, 0.8$ and 1.2 GW/cm^2 (marked as 1-5). (b) The same as in panel (a) for transmission coefficient. (c) Averaged over pulse absorption versus S [dashed curve is correspondent to Eq. (9)]. (d) The same as in panel (c) for transmission coefficient.

The temporal evolution of $\xi_{\Omega t}$ and $T_{\Omega t}$ at frequency Ω (solid and dotted curves are correspondent to the two recombination cases under consideration) are plotted in Figs. 5a and 5b. By analogy with Sect. IVA, the negative absorption regime takes place at $S \geq 0.3 \text{ GW/cm}^2$. Beside of this, the conditions $\xi_{\omega t} < 0$ take place around the peak positions at $\omega < \Omega$ (not plotted, see a similar behavior in Fig. 3a); for the first and second peaks the negative absorption regime is realized up to $t \sim 5\tau_p$ at $S \geq 0.1 \text{ GW/cm}^2$. In addition, at $t < 0.5\tau_p$ the response does not depend on recombination and at $t > 1.5\tau_p$ a damping or time-independent response is realized for the effective or suppressed recombination.

The averaged according to Eq. (7) absorption and transmission coefficients, which do not depend on the recombination mechanism, are plotted in Figs. 6c and 6d. Once again, ξ_S and T_S can be fitted by Eqs. (10) with the characteristic intensity $\bar{S} \approx 0.56 \text{ GW/cm}^2$ and the coefficient $h \approx 0.03 \text{ cm}^2/\text{GW}$. Since the departure rate from the photoexcited peak increases if $\hbar\Omega$ grows, the characteristic intensity \bar{S} is also increased in the visible spectral region in comparison with the near-IR pumping case.

V. DISCUSSION AND CONCLUSIONS

To summarize, we have developed the nonlinear theory of transient response of an intrinsic graphene under

the ultrafast interband excitation. Within the local time approach, the conditions of saturation of absorption were found in the mid-IR, near-IR, and visible spectral regions. In addition, we have demonstrated a possibility for the stimulated mid-IR radiation due to the bottleneck effect during the cascade emission of optical phonons. Our consideration is based on the set of assumptions about relaxation mechanisms. First of all, the phenomenological model for the broadening with the characteristic energy γ is used for description of the intersubband transitions. In Sects. III and IV we estimated γ from the experimental data for the departure relaxation rates. [1, 2, 9] Secondary, a simplified description of energy relaxation is employed. We neglect the Coulomb scattering which is not a dominant relaxation channel at $t \lesssim \tau_p$, so that the results for ξ_S and T_S should not be modified essentially. But a transient distribution at $t \gg \tau_p$ and a condition for the negative absorption of a probe radiation in the mid-IR region can be modified. Also, a possible contribution of the substrate vibration [12] is not taken into account. These points require a special consideration but, anyway, our calculation gives a lower bound of S . The other assumptions (parameters for the electron-phonon coupling, conditions for the temporally-local approach, and description of the interband response) are rather standard for the calculations of the optical properties and the relaxation phenomena in graphene. In addition, an inhomogeneity of pumping, which causes the lateral diffusion of carriers, [13] and a heating of phonons [14] may be essential; these phenomena require a special treatment, both experimental and theoretical.

We turn now to discussion of the experimental data available for the near-IR spectral region. [5, 6] Numerical estimates for the saturation thresholds and for the concentrations of the photoexcited carriers are in a qualitative agreement with the consideration performed. But an accurate comparison with the results presented is not possible for the two reasons. First, the graphene structure was embedded into the laser cavity in [5, 6] so that the electro-dynamical conditions (for a propagated, reflected, and absorbed radiation) were different from the simple geometry considered here. Second, the multi-layer graphene or the graphene flakes were used, while a single-layer graphene case was not under a detailed treatment. Thus, a special measurements with the use of the simplest geometry of a well-characterized sample placed over a semi-infinite substrate are necessary.

In closing, we have analyzed theoretically the conditions for realization of an efficient graphene-based saturable absorber and have performed a comparison with the experimental data. More extended treatment of this phenomena under near-IR pumping, including an above-mentioned special measurements, in order to improve an efficiency of the graphene based saturable absorber in the lasers for telecommunications. An additional study in the mid-IR and visible spectral regions should be useful for verification of different relaxation mechanisms.

The author would like to thank E. I. Karp for insightful comments.

Appendix: Rabi oscillations regime

Below we describe the saturation of the averaged absorption and transmission coefficients (7) under an ultrafast pumping for the case when the Rabi oscillations conditions are satisfied. [4] The collisionless regime of response is described by the S -dependent contribution to the distribution function

$$1 - 2f_{pt} = \cos \left(\sqrt{\frac{S}{S_R}} \int_{-\infty}^t \frac{dt'}{\tau_p} w_{t'} \right). \quad (\text{A.1})$$

Here the characteristic intensity is given by

$$S_R = \frac{\sqrt{\epsilon} c}{4\pi} \left(\frac{\hbar \Omega}{e \tau_p v} \right)^2 \quad (\text{A.2})$$

and $S_R \simeq 0.6$ MW/cm² for CO₂ pumping with $\tau_p \simeq 0.1$ ps. For the near-IR or visible pumping with $\tau_p \simeq 30$ fs, one obtains $S_R \simeq 0.3$ or 1 GW/cm². Notice, that $S_R \propto (\Omega/\tau_p)^2$ and (A.1) is not dependent on any other parameter if τ_p is shorter than the dephasing relaxation time.

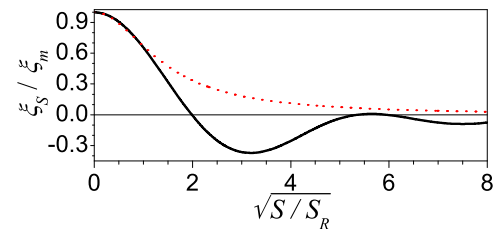


FIG. 7: (Color online) Normalized absorption coefficient given by (A.3) versus dimensionless intensity S/S_R . Dotted curve presents a monotonic fit.

Substituting the distribution (A.1) into Eqs. (6) and (7) one obtains the following analytical expression for the relative absorption

$$\frac{\xi_S}{\xi_m} = \int_{-\infty}^{\infty} \frac{dt}{\tau_p} w_t^2 \cos \left(\sqrt{\frac{S}{S_R}} \int_{-\infty}^t \frac{dt'}{\tau_p} w_{t'} \right) \quad (\text{A.3})$$

while the transmission coefficient is given by $T_S \approx T_m(1 - \tilde{a}\xi_S)$ with $\tilde{a} = \sqrt{\epsilon}(1 + \sqrt{\epsilon})/2$. In Fig. 7 we plot the function ξ_S/ξ_m versus dimensionless intensity S/S_R and the oscillating character of response at $S/S_R \geq 4$. The oscillations appears due to the dynamic inversion of transient population, see Ref. 4. The fit of (A.3) at $S/S_R \leq 1$ is given by Eq. (10) with the characteristic intensity $\bar{S} = 2S_R$.

-
- [1] J. M. Dawlaty, S. Shivaraman, M. Chandrashekhara, F. Rana, and M. G. Spencer Appl. Phys. Lett. **92**, 042116 (2008); D. Sun, Z.-K. Wu, C. Divin, X. Li, C. Berger, W. A. de Heer, P. N. First, and T. B. Norris, Phys. Rev. Lett. **101**, 157402 (2008); R. W. Newson, J. Dean, B. Schmidt, and H. M. van Driel, Opt. Exp. **17**, 2326 (2009).
- [2] F. Rana, P. A. George, J. H. Strait, J. Dawlaty, S. Shivaraman, Mvs Chandrashekhara, and M. G. Spencer, Phys. Rev. B **79**, 115447 (2009); P. N. Romanets and F.T. Vasko, Phys. Rev. B **81**, 085421 (2010).
- [3] F.T. Vasko and O.E. Raichev, *Quantum Kinetic Theory and Applications* (Springer, N.Y., 2005).
- [4] P. N. Romanets and F.T. Vasko, Phys. Rev. B **81**, 241411 (2010).
- [5] Z. Sun, T. Hasan, F. Torrisi, D. Popa, G. Privitera, F. Wang, F. Bonaccorso, D. M. Basko, and A. C. Ferrari, ACS Nano **4**, 803 (2010); Z. Sun, D. Popa, T. Hasan, F. Torrisi, F. Wang, E. J. R. Kelleher, J. C. Travers, and A. C. Ferrari, Nano Research **3**, 653 (2010).
- [6] H. Zhang, D.Y. Tang, L.M. Zhao, Q. Bao, K.P. Loh, Opt. Express, **17** 17630 (2009); H. Zhang, D. Tang, R.J. Knize, L. Zhao, Q. Bao, K.P. Loh, Appl. Phys. Lett., **96**, 111112 (2010).
- [7] V. Ryzhii, M. Ryzhii, and T. Otsuji, J. Appl. Phys. **101**, 083114 (2007); A. Satou, F. T. Vasko, and V. Ryzhii, Phys. Rev. B **78**, 115431 (2008).
- [8] L.A. Falkovsky, Phys. Usp. **51** 887 (2008); M. V. Strikha and F.T. Vasko, Phys. Rev. B **81**, 115413 (2010).
- [9] N.M.R. Peres, Rev. Mod. Phys. **82**, 2673 (2010); F. T. Vasko and V. Ryzhii, Phys. Rev. B **76**, 233404 (2007); X. Hong, K. Zou, and J. Zhu, Phys. Rev. B **80**, 241415 (2009).
- [10] H. Suzuura and T. Ando, J. Phys. Soc. Japan, **77**, 044703 (2008); S. Piscanec, M. Lazzeri, F. Mauri, A. C. Ferrari, and J. Robertson, Phys. Rev. Lett. **93**, 185503 (2004).
- [11] D. Potter, *Computational Physics* (J. Wiley, London, 1973).
- [12] J. H. Chen, C. Jang, S. Xiao, M. Ishigami, and M. S. Fuhrer, Nature Nanotech. **3**, 206 (2008); S. Fratini and F. Guinea, Phys. Rev. B **77**, 195415 (2008).
- [13] B. A. Ruzicka, S. Wang, L. K. Werake, B. Weintrub, K. P. Loh, and H. Zhao, arXiv:1005.3850.
- [14] C. H. Lui, K. F. Mak, J. Shan, and T. F. Heinz, Phys. Rev. Lett. **105**, 127404 (2010); H. Wang, J. H. Strait, P. A. George, S. Shivaraman, V. B. Shields, Mvs Chandrashekhara, J. Hwang, F. Rana, M. G. Spencer, C. S. Ruiz-Vargas, and J. Park, Appl. Phys. Lett. **96**, 081917 (2010).